



Citation for published version:

Drougkas, A, Verstryngge, E, Szekér, P, Heirman, G, Bejarano-Urrego, L, Giardina, G & Van Balen, K 2019, 'Numerical Modeling of a Church Nave Wall Subjected to Differential Settlements: Soil-Structure Interaction, Time-Dependence and Sensitivity Analysis', *International Journal of Architectural Heritage*.
<https://doi.org/10.1080/15583058.2019.1602682>

DOI:

[10.1080/15583058.2019.1602682](https://doi.org/10.1080/15583058.2019.1602682)

Publication date:

2019

Document Version

Peer reviewed version

[Link to publication](#)

This is an Accepted Manuscript of an article published by Taylor & Francis in *International Journal of Architectural Heritage* on 14 April 2019, available online:
<http://www.tandfonline.com/0.1080/15583058.2019.1602682>

University of Bath

General rights

Copyright and moral rights for the publications made accessible in the public portal are retained by the authors and/or other copyright owners and it is a condition of accessing publications that users recognise and abide by the legal requirements associated with these rights.

Take down policy

If you believe that this document breaches copyright please contact us providing details, and we will remove access to the work immediately and investigate your claim.

1 **Numerical Modeling of a Church Nave Wall Subjected**
2 **to Differential Settlements: Soil-Structure Interaction,**
3 **Time-Dependence and Sensitivity Analysis**

4 **Anastasios Drougkas¹**

5 Building Materials and Building Technology Division, Civil Engineering Department, KU Leuven,
6 Kasteelpark Arenberg 40 Box 2448, B-3001 Heverlee, Belgium

7 **Els Verstrynghe**

8 Building Materials and Building Technology Division, Civil Engineering Department, KU Leuven,
9 Kasteelpark Arenberg 40 Box 2448, B-3001 Heverlee, Belgium

10 **Pepijn Szekér**

11 Building Materials and Building Technology Division, Civil Engineering Department, KU Leuven,
12 Kasteelpark Arenberg 40 Box 2448, B-3001 Heverlee, Belgium

13 **Gert Heirman**

14 Triconsult nv, Lindekensveld 5 box 3.2, B-3560 Lummen, Belgium

15 **Leidy-Elvira Bejarano-Urrego**

16 Building Materials and Building Technology Division, Civil Engineering Department, KU Leuven,
17 Kasteelpark Arenberg 40 Box 2448, B-3001 Heverlee, Belgium

¹ Corresponding author, email: anastasios.drougkas@kuleuven.be

18 **Giorgia Giardina**

19 Department of Architecture and Civil Engineering, University of Bath, Claverton Down, Bath, BA2 7AY,
20 United Kingdom

21 **Koenraad Van Balen**

22 Building Materials and Building Technology Division, Civil Engineering Department, KU Leuven,
23 Kasteelpark Arenberg 40 Box 2448, B-3001 Heverlee, Belgium

24 **Abstract**

25 Historic masonry structures are particularly sensitive to differential soil settlements. These settlements may be
26 caused by deformable soil, shallow or inadequate foundation, structural additions in the building and changes in
27 the underground water table due to the large-scale land use change in urban areas.

28 This paper deals with the numerical modeling of a church nave wall subjected to differential settlement caused
29 by a combination of the above factors. The building in question, the church of Saint Jacob in Leuven, has suffered
30 extensive damage caused by centuries-long settlement. A numerical simulation campaign is carried out in order to
31 reproduce and interpret the cracking damage observed in the building.

32 The numerical analyses are based on material and soil property determination, the monitoring of settlement in
33 the church over an extended period of time and soil-structure interaction. A sensitivity study is carried out, focused
34 on the effect of material parameters on the response in terms of settlement magnitude and crack width and extent.
35 Soil consolidation over time is considered through an analytical approach. The numerical results are compared
36 with the in-situ observed damage and with an analytical damage prediction model.

37 **Keywords**

38 Masonry; soil-structure interaction; historic structures; finite element modeling; settlement-induced damage

39 **Highlights**

- 40 • A masonry church nave wall subjected to differential settlements is numerically modeled, considering
- 41 time-dependent material properties combined with changes in geometry and loading
- 42 • The foundation and the soil properties are directly considered
- 43 • A sensitivity analysis highlights the parameters affecting the cracking pattern and extent
- 44 • The phased analysis results in a much more accurate representation of the observed damage compared
- 45 to a single-phase model
- 46 • An analytical model for the calculation of damage due to differential settlements is expanded and
- 47 compared to the finite element analysis results

48 **Notation**

49	E	Young's modulus
50	G	shear modulus
51	ν	Poisson's ratio
52	ρ	mass density
53	σ_t	tensile stress
54	ε_{cr}	crack strain
55	ε_u	ultimate strain
56	f_c	compressive strength
57	f_t	tensile strength
58	G_f	tensile fracture energy

59	h	characteristic finite element length
60	L^j	footing half-length
61	B^j	footing half-width
62	D^j	footing embedment depth
63	A_f^j	footing area
64	A_w^j	footing side-wall contact area
65	K_n^j	footing vertical elastic stiffness
66	k_n^j	footing modulus of subgrade reaction
67	k_n	wall/colonnade modulus of subgrade reaction

68 **1. Introduction**

69 **1.1 State of the Art**

70 The analysis of large monumental structures subjected to differential ground movement is a challenging
71 subject of study. The challenge mainly arises from geometric complexity and sheer size, problems only partially
72 mitigated by a detailed geometric survey, material property determination and the definition of the applied
73 deformation load profile through concerted monitoring efforts [1]. It is, however, a worthwhile endeavor in service
74 of estimating the risk of damage or collapse and designing effective intervention strategies for repair and
75 strengthening.

76 The discretization of monumental church structures in macro-elements with different stiffness is often
77 considered conceptually and empirically valid. Macro-elements, such as façades, towers, apses and single naves,
78 are often separated through insufficient tying and the presence of structural cracking. They are further

79 characterized by different stiffness, weight and internal stresses. Namely, the effects of earthquake action and
80 differential settlement loading affect different parts of the structure in distinct ways. Therefore, the problem of
81 structural analysis of large churches can be simplified by pursuing it on an individual macro-element basis [2]. It
82 is both practical and valid to study certain components of monumental church structures, such as single bays,
83 naves, façades or towers individually.

84 In a nonlinear finite element (FE) analysis framework, the large dimensions of monumental church structures
85 built in masonry can render detailed modeling computationally prohibitive and model preparation effort excessive.
86 As an alternative to nonlinear FE modeling, rigid block analysis has been shown to be capable of reproducing
87 failure modes in masonry structures subjected to large movement of their supports [3,4]. When failure is mostly
88 concentrated in the joints, either through sliding and/or opening, as is the case in dry joint masonry and, usually,
89 in masonry with weak lime mortar joints, rigid block analysis becomes an attractive approach. However, sheer
90 size and geometrical complexity, due to an irregular bond and the existence of multiple masonry leaves, render
91 such approaches difficult to implement in large structures. Macro-modeling, therefore, which consists in the
92 homogenous modeling of the masonry composite, becomes a more suitable alternative. Despite the assumption of
93 homogeneity, nonlinear macro-modeling of large masonry structures can provide insight into the mechanisms
94 through which damage arises and expands [5,6].

95 Predictive models for damage estimation and categorization in masonry structures subjected to differential
96 ground movement have been proposed in the literature [7–9]. These models rely on the determination of
97 parameters related to the material, geometric and foundation properties of the structure and are mostly used to
98 evaluate the effects of tunneling-induced settlements. The loading parameters for these models can be determined
99 using terrestrial or space-borne means, comparing the differential settlement to empirical, semi-empirical or
100 calculated limits for the determination of the level of damage. The analytical and parametric basis of these models
101 allows their adoption and modification according to the requirements of a variety of loading scenarios and
102 foundation types. The application spectrum of such methods extends from damage prediction in individual

103 buildings to vulnerability assessment in entire urban aggregates. This basis further allows the parallel application
104 with, and direct comparison to, numerical modeling of damage induced by differential ground settlement.

105 In this paper both numerical and analytical models are applied for the analysis of a large monumental structure.
106 The church of Saint Jacob in Leuven has been the subject of wide and inclusive study over the preceding decades
107 [10–12]. It is characterized by extensive and developing damage due to differential ground movement. This
108 damage is well documented and extensive data is available on the profile of ground movement over different
109 periods. Finally, studies have been performed on its material properties, the stress state of its structural elements
110 and the properties of the foundation soil. It is therefore a prime candidate for investigation through analytical
111 simulation and numerical analysis for the purpose of interpreting the damages present in the fabric and the
112 development of ground movement.

113 **1.2 Objectives**

114 The focus of the present paper is the numerical reproduction of the damage patterns observed over time in the
115 church of Saint Jacob in Leuven, the investigation of their underlying cause, namely the differential settlements at
116 the site, and the study of the effect of material and numerical analysis parameters in the obtained results. This is
117 accomplished through a sensitivity study involving the material properties of the masonry structure, the application
118 of different loading patterns in the form of settlement profiles and the variation of the boundary conditions as
119 affected by the passage of time.

120 The interpretation of the results of the numerical analyses, coupled with the assembly and evaluation of historic
121 data, on-site observations and structural monitoring aim at providing insight into the occurrence and development
122 of structural damage in the monument. A quantitative assessment of the development in time of soil consolidation
123 under the effect of gravity loads is given, thus outlining the behavior of the monument over an extended period.

124 Further interpretation and quantification of the numerical results is provided through their comparison with
125 simplified analytical damage assessment models. This comparison allows the evaluation of the applicability of

126 analytical models in monumental masonry structures and demonstrates their potential for the interpretation of
127 current and the prediction of future structural damage.

128 **2. The Case Study**

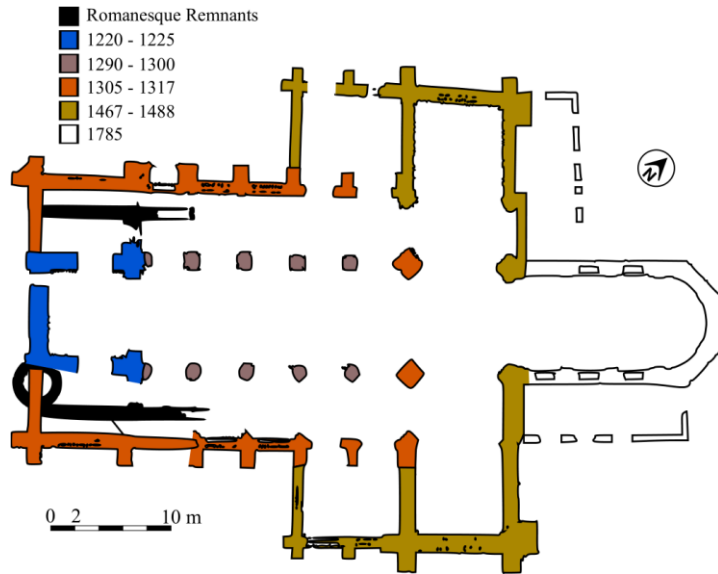
129 **2.1 Layout and Brief Historic Outline**

130 Details on the history of the construction of the church may be found in [10], with the main points repeated
131 here for clarity. Construction of St. Jacob's church began around 1220, with the erection of the tower over the
132 remnants of an existing Romanesque church. The initial plan called for the church to have a flat timber ceiling,
133 which was later substituted for a timber barrel vault. The main nave, at its originally intended height, was
134 completed in the 14th century, along with the side naves and their stone vaults, and the bell tower over the crossing
135 was added in the 15th. During the period 1534-1535, an additional level over the main nave was added and masonry
136 vaults were added in place of the timber vault, which was complemented by the addition of two, possibly four,
137 pairs of flying buttresses. These alterations resulted in the addition of self-weight not originally anticipated in the
138 construction of the foundations.

139 First mention of structural problems stemming from differential settlement dates back to at least the 15th
140 century. These problems led to the reconstruction of the side nave vaults. The timber bell tower over the crossing
141 was dismantled in 1735 due to concerns over its decay. The development of vertical cracking in the pillars led to
142 the installment of confining steel rings in the early 19th century, still present. Further consolidation measures were
143 taken in the early 20th century due to severe cracking in the west wall of the northern transept. In 1963, the entire
144 church was definitively closed for the public. During the partially executed consolidation works of 1965-1971, the
145 structure was internally shored using massive reinforced concrete elements and steel profile braces. While only
146 foreseen as a temporary measure, the shoring members are still present today. Additionally, the side nave vaults
147 were dismantled for weight reduction. In 2000 the flying buttresses were removed due to their being severely out-
148 of-plumb, which raised concerns of sudden collapse, and were replaced by temporary steel tie-rods. A
149 comprehensive structural intervention project, including localized repairs on the masonry a micro-piling

150 reinforcement of the foundations and reconstruction of the dismantled elements (side nave vaults and flying
151 buttresses) and soil consolidation was launched in September 2018 [13].

152 A floor plan of the church, along with the designation of the construction phases, can be seen in Figure 1. The
153 construction process, beginning with the tower and following with the arcade, naves, transept, chapels and finally
154 the choir are indicated.



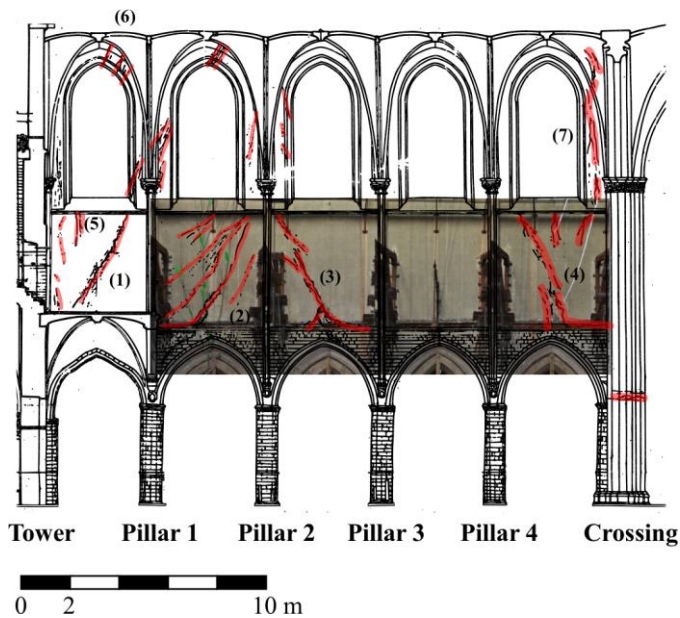
155
156 **Figure 1 Church floor plan and construction phases. Adapted from [10].**

157 2.2 Damage Survey

158 The differential settlements in the church, which are the cause of the clear majority of structural damage, are
159 caused by the building being erected in a swamp area near the river Voer, coupled with the initially unplanned
160 addition of a second and third level, resulting in a severe increase in self-weight. The substitution of the original
161 flat timber ceiling with a wooden barrel vault and, later, a masonry vault resulted in further increase in the self-
162 weight.

163 The present study focuses on the damage documented in the northern wall of the main nave. An elevation
164 view, the main structural elements and damage, along with the notation used for their designation, is shown in
165 Figure 2. The nave wall measures approximately 26 m in length and 21 m in height. The damage of the nave,

166 consisting primarily of cracks caused by differential settlement, has been documented both with hand drawings
167 and photographically during site visits, and more recently using semi-automated point-cloud data processing [14].



168

169 **Figure 2 Northern wall of main nave: structural element designation and documented major cracks**
170 **indicated in red (adapted from a hand-drawn survey of the building's geometry and pathology carried out**
171 **by students of the Raymond Lemaire International Centre for Conservation, 1983-1984 [15]). In underlay**
172 **a photographic survey of northern nave wall cracks. View of cracks above nave pillars (photo by Pepijn**
173 **Szekér, 2018).**

174 The arithmetically designated cracks 2 through 4 of the nave have been photographically documented and are
175 shown in underlay in Figure 2. Continuous visibility of cracks 1 through 4 is not possible due to the obstruction
176 caused by the organ loft near the western tower. Despite the time passed between the survey in 1983-1984 and
177 the photographic survey in 2018 (Figure 2), there does not appear to be any lengthening of the major cracks.
178 However, the same cannot be said with certainty about the crack widths, however, since these were not measured
179 in the prior case.

180 The widths of the cracks above the nave pillars have been measured by hand. While the external plaster
181 presents a crack width of a few mm, the crack width on the masonry behind the plaster is roughly between 10mm

182 and 20mm (i.e. eroded mortar joints), Figure 3. The cracks appear to mostly pass through the mortar joints rather
183 than splitting the masonry stone units in the investigated area.

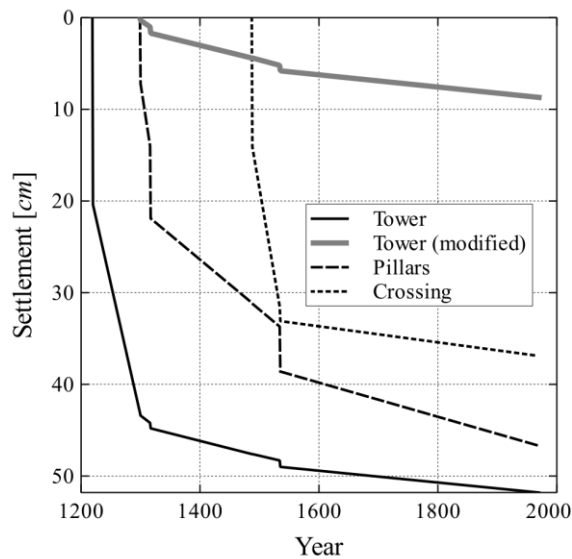


184

185 **Figure 3 Close-up of cracks 4 on main nave wall (photo by Els Verstrynge, 2018).**

186 **2.3 History of Settlements: Estimation and Geomatic Data Processing**

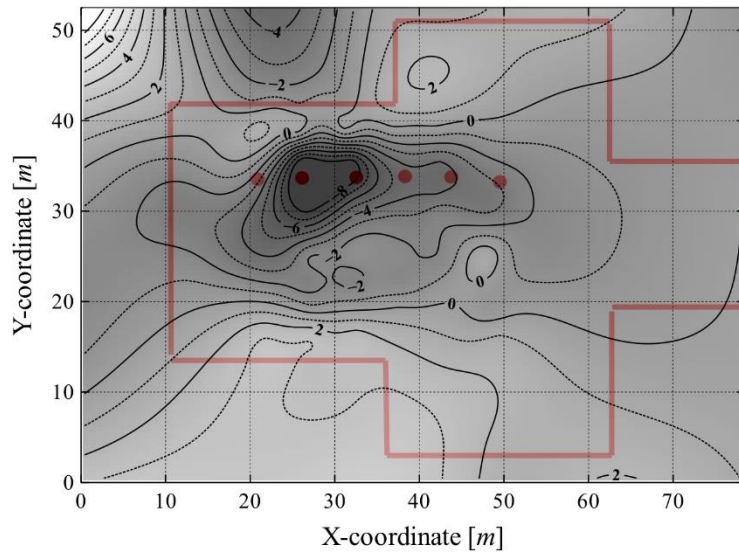
187 An estimation of the soil settlements for different parts of the structure, under different calculated loads, has
188 been carried out in the extensive studies of the church. These results are presented in internal technical reports,
189 property of KU Leuven [15]. These settlements are presented for the tower, crossing and pillars in Figure 4 and
190 have been calculated based on cone penetration tests and evaluation of the soil consolidation progress according
191 to Terzaghi, Buisman and Koppejan [16]. The results are not differentiated between individual pillars, thus
192 rendering the calculation of the differential settlement between pillars impossible. Since the tower was completed
193 before the beginning of the construction of the nave, an additional graph of the development of the tower settlement
194 is provided. This graph ignores the settlements occurred before the completion of the nave wall (see grey line in
195 Figure 4).



196

197 **Figure 4** Calculated settlements for different structural components of the tower and nave from 1220
 198 to 1970 (adapted from [15]).

199 Concerning more recent ground movement and the resulting differential settlement of the pillars, levelling
 200 surveys conducted over the previous two decades provide info on the development of differential settlements over
 201 selected periods of measurements. Contour plots of the settlements over the period 1994-2005 are presented in
 202 Figure 5. These geodetic survey results are presented in terms of settlement relative to a point in the choir which
 203 is considered, due to the absence of apparent damage, stable. The maximum settlement over this period was
 204 measured at the area around pillars 1 and 2 of the northern nave, with areas at the southern nave and northern
 205 transept presenting some uplifting. The settlement at pillars 1 and 2 is consistent with cracks 1, 2 and 3 as indicated
 206 in Figure 2, although the time of the first appearance of these cracks is not known with certainty. It is interesting
 207 to note that all points along the nave exhibited a rather uniform settlement in the period 1994-2000, while in the
 208 period 2000-2005 the settlement of pillar 2 appeared to increase at a faster rate than the other points in the nave.



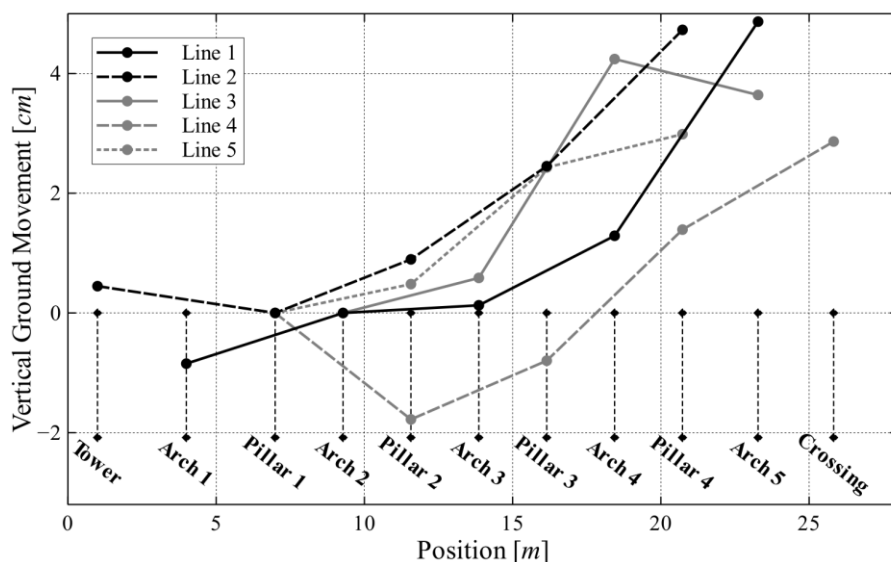
209

210 **Figure 5 Contour plot of ground settlement in mm during the period 1994-2005 against church**
 211 **architectural outline. Location of northern nave from tower pilaster to crossing indicated by solid hatch**
 212 **circles.**

213 An additional third approach may be adopted for the evaluation of the differential settlements over the entire
 214 history of the church. This is accomplished through the study of the geometric disposition of characteristic
 215 architectural features present on the structural elements. This approach is based on detailed laser scanning data
 216 acquired in the context of this investigation [14]. The downside of this rough approach is the inability to evaluate
 217 the total settlement that each element has undergone: only the final differential settlement can be estimated. Five
 218 reference features are chosen for this approach, from top to bottom: 1) the top of the third level arches' voussoirs,
 219 2) the base of the pilaster abacus of the third level, 3) the top of the first level arches' voussoirs, 4) the base of the
 220 pillar abacus of the first level and 5) the top of the first level pillar pedestals. Assuming that features 1-2, and
 221 similarly 3-4-5, were built at the same period, it follows that they were, in all probability, vertically level at the
 222 time of construction.

223 The measured vertical displacements relative to pillar 1 (lines 2, 4-5) or arch 2 (lines 1, 3) are shown in Figure
 224 6. All architectural features are present in pillar 1 and its neighboring arch span, hence the choice of these elements
 225 as a reference, instead of, for example, the crossing column. The obtained profile is similar to the profile found in

226 the recent leveling measurements, with the settlement being mostly concentrated around pillars 1 and 2. This is
 227 consistent with the formation of cracks 2 and 3 (Figure 2). Differences in the profile at different heights of the
 228 structure are expected for two reasons: a) differential settlement generally affects the lower parts of the building
 229 more severely and b) the second and third levels of the nave wall were constructed at a later phase, when part of
 230 the settlements of the colonnade had already occurred.



231

232 **Figure 6 Differential settlements relative to pillar 1 (position: 6.99 m) measured from point cloud**
 233 **data architectural feature analysis. Position distance measured from tower pilaster.**

234 3. Analysis Procedure

235 3.1 Modeling the Nave Wall

236 The geometry of the nave is derived from an idealization of the in-situ geometry in its undeformed state. A
 237 distinction is made between the three-leaf masonry of the nave wall and the solid stone masonry of the lower part
 238 of the pillars, each with its own set of material properties. The basic values of the material properties used for the
 239 numerical analyses, in part determined in previous experimental efforts [10,11] and in part assigned nominal or
 240 empirical values as proposed in the relevant literature [17,18], are summarized in Table 1.

241 **Table 1 Basic material properties used in numerical analysis.**

	E [N/mm ²]	ν [-]	ρ [kg/m ³]	f_c [N/mm ²]	f_t [N/mm ²]	G_f [N/mm]
Wall masonry	3000 ^c	0.15 ^c	1920 ^b	6.99 ^a	0.10 ^c	0.012 ^d
Pillar masonry	15700 ^b	0.20 ^b	2360 ^b	11.95 ^a	1.00 ^d	0.075 ^d
	a: experimentally derived value [10]			c: estimated value [17]		
	b: experimentally derived value [11]			d: estimated value [18]		

242 The masonry walls and columns of the nave are modeled using 8-node quadrilateral and 6-node triangular
 243 plane stress elements, an approach suited to the geometric arrangement, element thickness and load orientation. A
 244 macro-modeling approach is adopted for the model, in which the masonry composite is treated as a homogenous
 245 continuum, with no distinction between units, mortar and the unit-mortar interface. The nonlinearity in tension is
 246 modeled using a multi-directional fixed crack model [19]. The model is based on a decomposition of the total
 247 tensile strain into an elastic and a crack component. The crack strain is further decomposed, allowing for the
 248 formation of a number of cracks simultaneously. A Rankine-type tension cut-off is used in pure or biaxial tension,
 249 while the influence of lateral compression is accounted for through a Mohr-Coulomb-type criterion. Nonlinear
 250 tension softening is assumed, governed by fracture energy, according to the expression:

$$\sigma_t = \begin{cases} f_t \left(1 - \frac{\varepsilon_{cr}}{\varepsilon_u}\right)^{0.31} & \text{for } 0 \leq \varepsilon_{cr} \leq \varepsilon_u \\ 0 & \text{for } \varepsilon_u \leq \varepsilon_{cr} < \infty \end{cases} \quad (1)$$

251 where σ_t is the tensile stress, ε_{cr} is the crack strain and ε_u is the ultimate strain, calculated according to the
 252 expression [20]:

$$\varepsilon_u = 4.226 \frac{G_f}{f_t h} \quad (2)$$

253 where h is the characteristic length of the finite element. The fracture energy/characteristic length approach
 254 results in mesh objectivity, provided the element length is sufficiently small to avoid a constitutive snap-back. The

255 maximum size criterion, based on the requirement for the initial tangent of the tensioning softening diagram to be
256 less than the Young's modulus, is satisfied for the chosen element length.

257 While the nave cracks appear to be mostly developed along the joints and not through the units. A detailed
258 modeling approach based on rigid-block or block-joint models could potentially be employed. However, the
259 dimensions of the structure are prohibitive for such detail to be practical. The geometric survey would need to
260 include detailed information on the dimension and arrangement of the outer leaf stones. Further, even if nominal
261 dimensions and a regular pattern were adopted, the infill would still need to be individually modeled. Macro-
262 modeling was therefore adopted as a practical solution, nevertheless capable of providing sufficiently detailed
263 results for the purposes of the paper.

264 The steel rings installed in the 19th century were not included due to the lack of data on their material properties
265 and state of decay. It is not expected, however, that this omission affects the cracking of the nave walls to any
266 significant extent.

267 **3.2 Foundation and Soil-Structure Interaction**

268 Soil-structure interaction is directly considered through the introduction of linear elastic structural interfaces
269 at the base of the masonry pillars, capable of accounting for normal and shear deformation. The normal stiffness
270 may be determined according to two distinct approaches: (a) from a calibration effort targeted at reproducing the
271 settlement profile measured over a given time period and (b) directly from the geometric characteristics of the
272 pillar footing and the elastic properties of the soil.

273 Both approaches are adopted and compared in the present paper. The values obtained from approach (a) are
274 presented in the results section. For approach (b), the vertical elastic spring constant for a single rigid arbitrarily
275 shaped footing j circumscribed in a rectangle with dimensions $2L^j \cdot 2B^j$ and embedded in the ground at a depth
276 of D^j is equal to [21]:

$$K_n^j = \frac{2GL^j}{1-\nu} (0.73 + 1.54x^{0.75}) \left[1 + \frac{1}{21} \frac{D^j}{B^j} (1 + 1.3x) \right] \left[1 + 0.2 \left(\frac{A_w^j}{A_f^j} \right)^{2/3} \right] \quad (3)$$

277 where G is the shear modulus of the soil, ν is the Poisson's ratio of the soil, A_f^j is the area of the footing, A_w^j
 278 is the total sidewall-soil contact area (equal to the perimeter of the footing times the embedment depth D^j in case
 279 of a foundation with constant cross-section) and $x = A_f^j / (2L^j)^2$. Division of the spring constant by A_f^j produces
 280 the modulus of subgrade reaction for a single footing:

$$k_n^j = \frac{K_n^j}{A_f^j} \quad (4)$$

281 This value is used for the normal stiffness of the interfaces below the pillars, adjusted according to the ratio of
 282 the base area of the footing over the cross-sectional area of the pillar at ground level. The settlement d_n^j of the
 283 foundation for a given normal force F_n^j is:

$$d_n^j = \frac{F_n^j}{K_n^j} \quad (5)$$

284 The value for the shear stiffness of the interface is calculated by the expression:

$$k_s^j = \frac{k_n^j}{2(1+\nu)} \quad (6)$$

285 according to the Poisson's ratio ν of the stone masonry foundation. This value is not determined
 286 experimentally but is consistent with the material properties of the stone masonry and is numerically more stable
 287 and less arbitrary than the use of a dummy value that precludes shear slipping at the foundation. This slipping

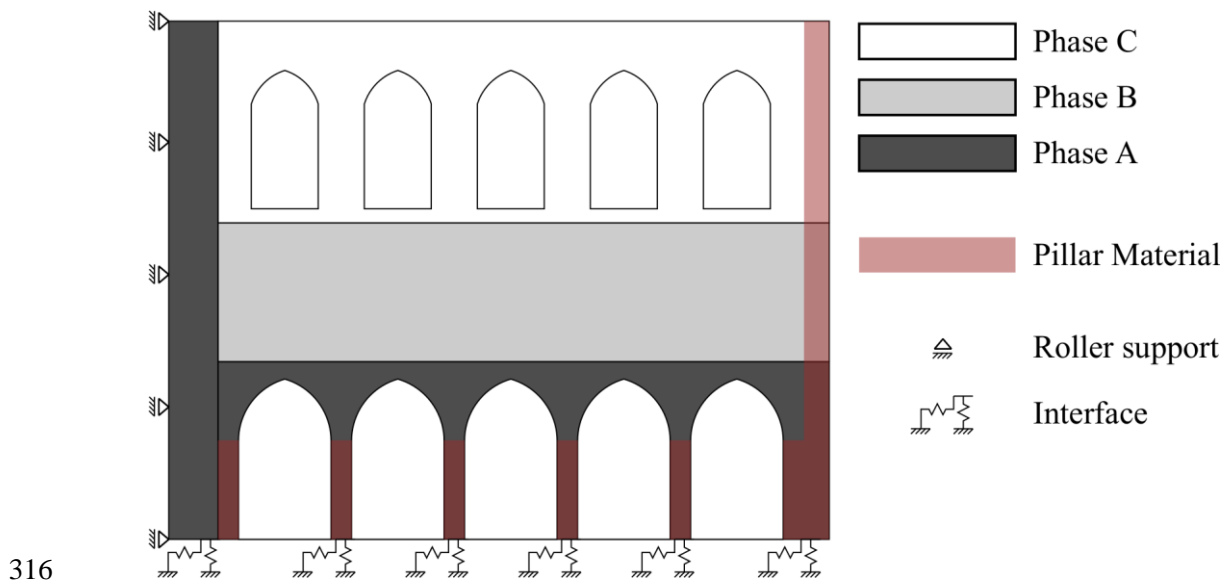
288 mode is, in any case, constrained by the high compressive stress applied on the interface by the self-weight and
289 the lack of horizontal loads. Therefore, the shear stiffness is calculated for a Poisson's ratio of 0.20 without further
290 investigation.

291 The soil beneath the church foundations has been investigated and found to be generally composed of, from
292 the surface advancing in depth: a) sandy clay (± 2.0 m thick), b) highly compressible peat (± 2.0 m thick), c) sandy
293 clay (± 2.6 m thick), d) quaternary clay-containing sand (± 5.4 m thick) and e) tertiary highly consolidated clay-
294 containing sand (unknown thickness) [10]. The foundation bases of the main pillars are roughly in the middle of
295 the peat layer. In the present case study, the settlements have been calculated prior to this investigation. Therefore,
296 the interface normal stiffnesses can be directly calculated from eq. (5) and (4). Using eq. (3) the apparent Young's
297 modulus of the homogenized foundation soil can be back-calculated. In the case of the nave pillars at the final
298 settlement (as shown in Figure 4) this apparent Young's modulus is equal to 0.597 N/mm^2 or 2.400 N/mm^2
299 when taking into account or disregarding the effect of embedment respectively. The former value is representative
300 of peats, while the latter is rather low for the all the soils in the other layers. This indicates the major contribution
301 of the peat layer to the total settlements and the potential primary cause of the excessive settlements of the church
302 at the nave.

303 For all analysis cases, the structure is let to deform under its self-weight and the extra load applied at various
304 levels of the nave wall from other elements present in the structure but not explicitly modeled, such as the timber
305 roof or the stone masonry vaults.

306 All finite element calculations were carried out using the DIANA FEA package [22]. The geometric layout
307 and the boundary conditions applied are illustrated in Figure 7. The different phases are colored in shades of grey
308 and the areas where pillar masonry material is assigned are given a reddish overlay. It is assumed that the tower to
309 the west of the nave (left side in the illustration) provides a rigid lateral support to the nave. This assumption is
310 based on the greater bending stiffness of the tower, due to greater foundation depth, better preservation state, wall
311 thickness and closed box plan, compared to that of the nave wall. It is further assumed that the nave wall is not
312 constrained towards the crossing in the east. This assumption, in turn, is based on the connection to the transept

313 being effected by the vaults, which cannot provide significant constraint to a solid masonry wall. The average
314 element length is roughly 166 mm, resulting in a total of 40308 nodes and 13029 continuum and 37 interface
315 elements. The roof loads associated with each of the three phases is applied at the top of every model.

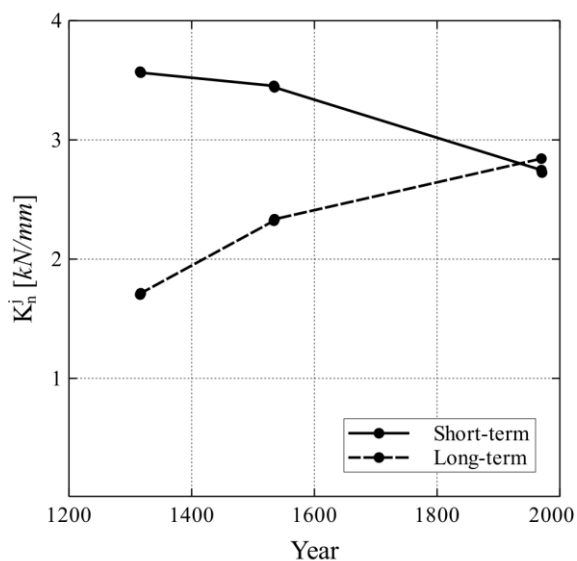


316
317 **Figure 7 Geometric layout of church nave wall. Structural phase designation, boundary conditions**
318 **and material assignment.**

319 3.3 Definition of Time Periods for Phased Analysis

320 Three different time periods are defined for the investigation of the time-dependent behavior of the building:
321 period A (1300-1316), period B (1317-1534) and period C (1535-1970), which coincide with the construction
322 phases illustrated in Figure 7. The beginning of period A corresponds to the completion of the first nave wall level.
323 The end of period A corresponds to the initiation of the increase of the height of the nave and period B starts upon
324 its completion. The end of period B corresponds to the construction of the crossing and the third level of the nave
325 wall. Period C brings us near to the present period, at the time of major temporary shoring of the building. The
326 analysis period covers the entire history of the monument up to before the point of internal shoring. The post-
327 intervention state of the monument will be a subject of further study in the future.

328 Through use of the equations (3) to (5), and for known values of the applied force and displacement, one may
 329 calculate the normal interface stiffness, and also back-calculate the apparent Young's modulus of the soil at given
 330 time instants. Both the forces and the settlements have been estimated for various points in the history of the
 331 building, as shown in Figure 4. The calculated normal interface stiffness for different structural parts through time
 332 is shown in Figure 8. This value is proportional to the apparent Young's modulus of the soil. One can differentiate
 333 between a short-term Young's modulus, governed by immediate settlements due to a change in load, and a long-
 334 term Young's modulus, governed by settlements due to, for example, consolidation. In the case of the pillars, the
 335 short-term Young's modulus generally exhibits a decreasing trend, whereas the long-term modulus exhibits an
 336 increase. The two curves appear to converge near the end of the measurement period, indicating that processes
 337 causing settlement under sustained loads have been halted. The consolidation being further completed accounts
 338 for the latter phenomenon, but the continuation of the settlements cannot be entirely excluded.



339

340 **Figure 8** Calculated pillar spring stiffness for estimated loads and settlements. Development of
 341 instant and long-term response.

342 **3.4 Analysis Approaches**

343 Three different approaches will be adopted for the analysis of the nave: a single-phase analysis, a phased
 344 analysis and a parametric study.

345 Firstly, in the single-phase analysis, the whole structure is taken in its entirety and the foundation interfaces
346 are assigned their final values according to the estimated settlements of each structural part and the dimensions of
347 the footings.

348 Secondly, in the phased analysis, three major phases are considered, with each one decomposed into two parts.
349 The major phases correspond to the phase designation indicated in Figure 7 and the decomposition of each phase
350 is based on the differences between the short-term (immediate) and the long-term response of the structure under
351 the sustained loads of each phase. Both the single-phase analysis and phased analysis make use of approach (b)
352 for determining the interface normal stiffness as explained in Section 3.2. In order to facilitate the conformity of
353 the previously and newly active parts of the mesh during the transition between phases, the structure was unloaded
354 in a stepwise manner before the activation of the new parts. This approach maintains the damage location and the
355 local reduction of stiffness due to cracking.

356 The self-weight is applied in 50 steps for each phase of all the analyses. A regular Newton-Raphson iteration
357 method is employed, with a 0.001 energy norm for convergence. Thirdly, a parametric analysis is performed to
358 address uncertainties in the mechanical properties of the materials. In order to reduce the computational cost, these
359 analyses are only carried out for the settlement profile obtained from the levelling surveys of the period 1994-
360 2005. Such analysis is defined in Section 3.2 as approach (a) for determining the normal stiffness. In the following
361 section, this choice of loading is motivated further, through a discussion of the obtained failure patterns. The
362 material parameters included in the investigation are the Young's modulus, the tensile strength and the tensile
363 fracture energy of the masonry composing the nave. The variation of the parameters ranged from 50% to 200% of
364 the initial values indicated in Table 1. The model using the initial values will be henceforth referred to as the
365 reference model.

366 4. Analysis Results

367 4.1 Single-Phase Analysis

368 As a first approach, the self-weight of the complete structure along with the final additional roof weights is
369 applied in a single phase. The final value for the stiffness of the foundation interfaces is used (see Figure 8),
370 corresponding to the long-term soil modulus of phase C. The obtained crack pattern is shown in Figure 9. The
371 obtained damage pattern presents several differences from the actual structure. Due to the settlement towards the
372 crossing, the response is dominated by the separation cracks between the nave and the tower. Crack 2 above arch
373 2 (Figure 2) is entirely absent. A single crack is formed between pillars 2 and 3 (crack 3, but inclined in the other
374 direction) and the crossing itself remains intact, as does its connection with the wall. Therefore, application of the
375 deformation loads in a single analysis step reveals only part of the response of the building and is not indicative
376 of its behavior throughout its history.



377

378 **Figure 9 Crack patterns for application of load in single analysis phase.**

379 4.2 Phased Analysis

380 The phased analysis of the nave provides a much more complete and detailed illustration of the development
381 of damage on the building throughout its history (Figure 10). The obtained settlement profiles derived from the
382 phased analysis, as well as from the single-phase case, are presented in Figure 11.

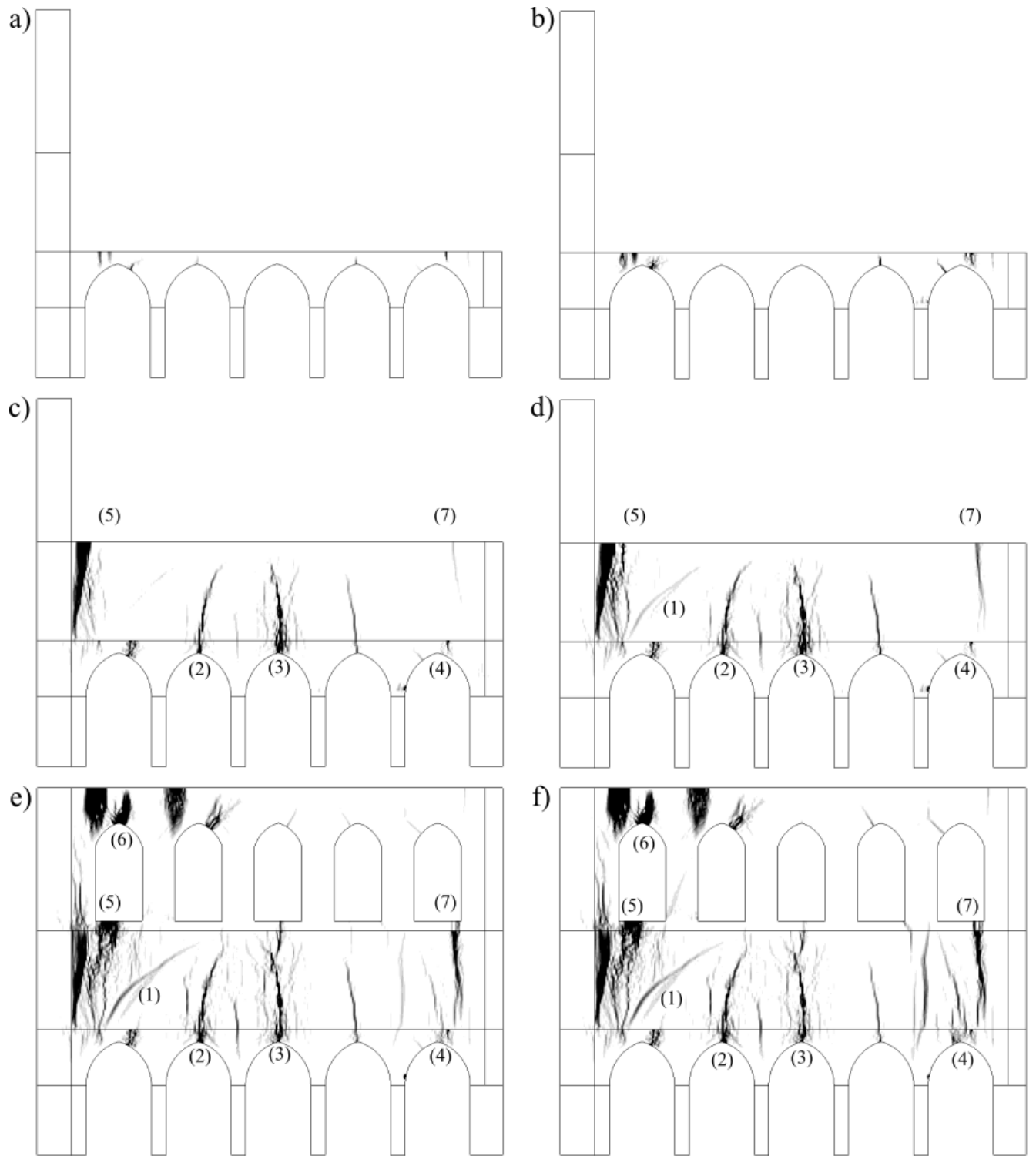
383 During phase A, only slight damage is registered at arches 1 and 5, see Figure 10a. There is some widening of
384 the cracks under long-term loading, but no formation of new major cracks, see Figure 10b. The response is mostly
385 of a sagging type due to the tower and the crossing exhibiting only minor settlement. Due to the numerical cracks
386 not having sufficiently developed in extent, no clear comparison between the numerically derived cracks and the
387 existing damage in the building can be made.

388 The situation changes significantly during phase B with the increase of the height of the nave wall above the
389 colonnade. A major separation crack is formed in the short-term phase between the tower and the nave (cracks 1
390 and 5). Additionally, cracks 2 and 3 are formed above pillar 3. At the end of the long-term loading, cracks 1 and
391 4 have emerged above the main colonnade. While the settlement profile is mostly of a sagging type at the end of
392 the short-term phase (Figure 11), a mixed profile with a significant tilting component is obtained at the end of the
393 long-term phase. The increase of the weight at the crossing is substantial and unable to be borne by its foundations.

394 Phase C witnesses the formation of the new cracks above and beside the third level windows (cracks 6 and 7
395 in Figure 2). The extent of the previously formed cracks is increased without, however, significant widening,
396 indicating the activation of the cracks at the new parts of the structure. As shown in Figure 11, the obtained profile
397 resembles the tilting-dominated response at the end of phase B, but of a larger magnitude.

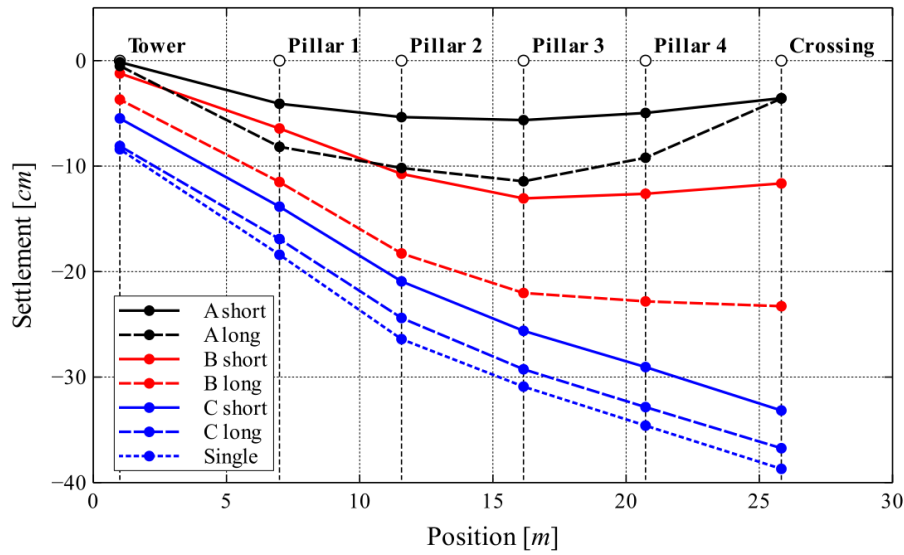
398 In Figure 11, the maximum settlement obtained at the end of the phase C closely resembles that of the single-
399 phase analysis, albeit with a slightly smaller magnitude. Nevertheless, the cracking pattern is significantly different
400 in the two approaches. The resulting cracking pattern from the phased analysis resembles in a higher degree the
401 actual pattern (compare Figure 2 and Figure 10). The cracking pattern resulting from the phased analysis resembles
402 much more closely the actual crack pattern compared to the single-phase analysis (compare Figure 9 and Figure
403 10). The complexity of the model, as the outcome of soil-structure interaction, is underlined by the substantially
404 different settlements obtained between the four pillars. This is despite the fact that they are of the same cross-
405 section with identical foundations (meaning equal interface stiffness) and bearing roughly the same vertical loads.

406 Overall, as time progresses, the deflection ratio of the structure tends to decrease, despite the increase in the
407 overall settlements (Figure 11). Cracks 2 and 3, caused by the sagging of the center are nearly fully developed by
408 the end of phase B, after which newly arising damage is possibly associated with tilting of the nave towards the
409 crossing. The maximum width of the cracks in the first level of the wall in fact decreases from phase B to phase C
410 due to the stabilizing effect of the added stiffness of the second level and despite the increase in weight.



411

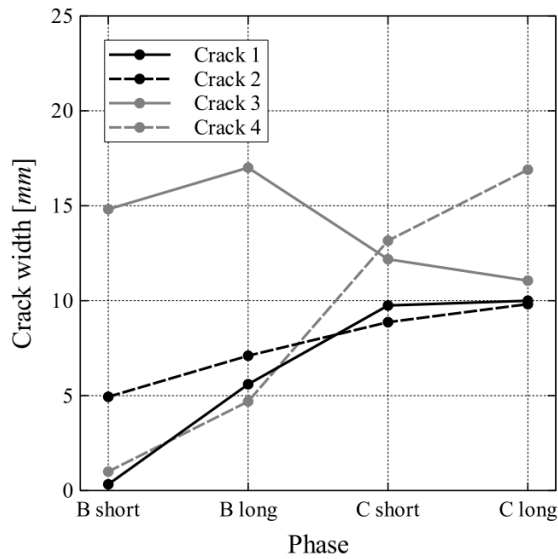
412 **Figure 10 Crack patterns for phased analysis of nave: a) phase A short-term, b) phase A long-term, c)**
 413 **phase B short-term, d) phase B long-term, e) phase C short-term, f) phase C long-term.**



414

415 **Figure 11 Settlement profiles obtained from finite element analysis: phased analysis and single-phase**
 416 **approaches.**

417 The numerically obtained cracks have been linked to cracks documented in the structure (Figure 2 and Figure
 418 10). Rather than integrating the obtained crack strains over the continuum to calculate the crack width, the opening
 419 of the cracks is indirectly calculated through measurement of the horizontal relative displacements of nodes on
 420 either side of the smeared crack mouth. Displacements due to elastic stress are minimal compared to displacements
 421 due to crack opening. In cases where the cracks in the actual structure are composed of more than one distinct
 422 branch, this measured numerical crack width is divided by the number of branches in order to obtain the magnitude
 423 of a single crack branch. The development of the normalized crack width, defined as the sum of the crack width
 424 divided by the number of crack branches in the actual structure, is presented in Figure 12. All cracks tend to
 425 increase with the passage of time, except crack 3, which is reduced in width after the construction of the second
 426 and third level of the nave.

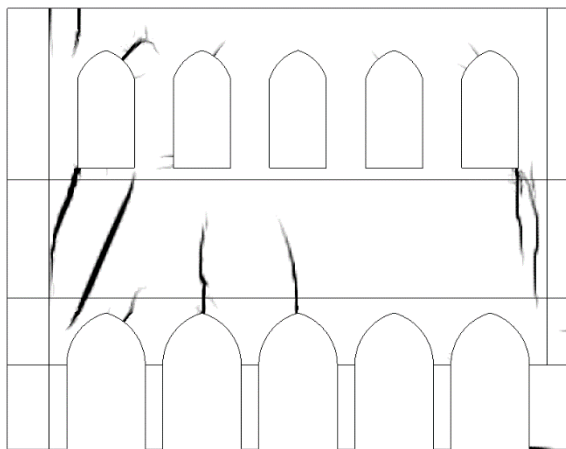


427

428 **Figure 12 Normalized crack width for various analysis phases.**

429 **4.3 Parametric Investigation**

430 The damage pattern obtained from the reference model is shown in Figure 13. This is the outcome of the
 431 application of the settlement pattern measured in the period 1994-2005. Rather than the displacement being applied
 432 to the supports directly, the stiffness of the interfaces was calibrated in order to match this settlement profile. This
 433 approach allows the evaluation of the soil-structure-interaction by altering the settlements from a variation of the
 434 stiffness of the superstructure.

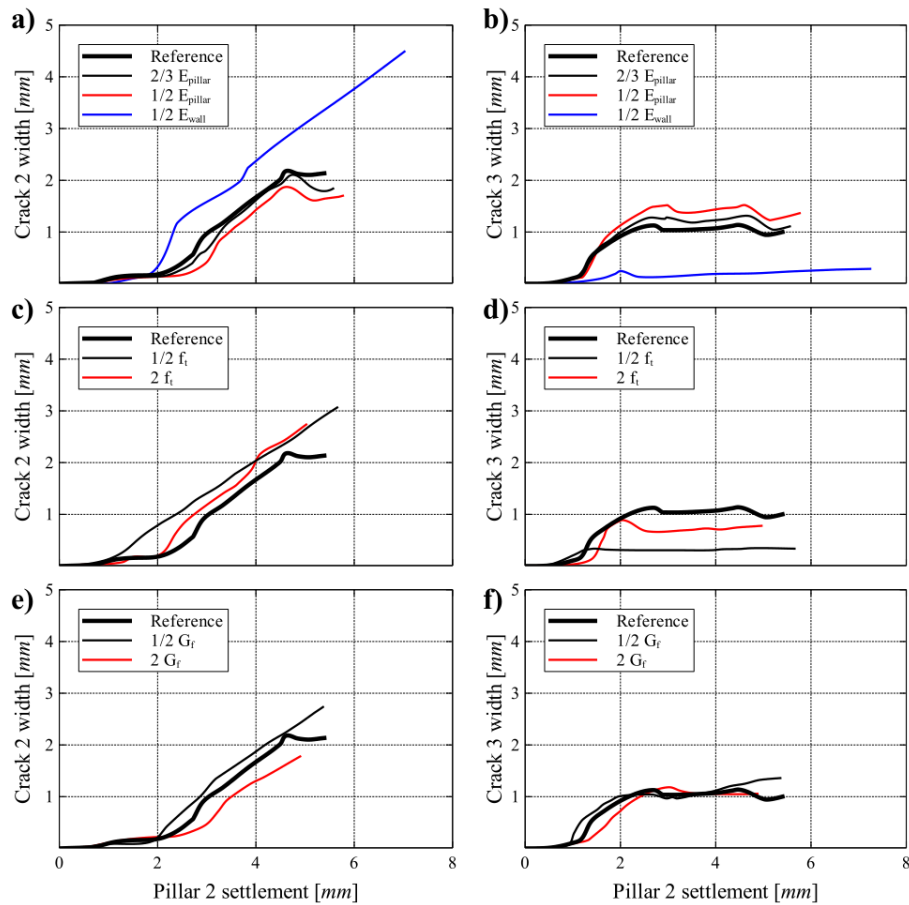


435

436 **Figure 13 Crack pattern obtained from the reference model of the parametric investigation.**

437 Despite the narrow extent of this measurement period compared to the entire history of the building, the
438 pattern closely resembles the damage present in the structure, both in location and extent, albeit with a much
439 smaller magnitude in terms of crack width. This constitutes an indication that the emergency measures taken from
440 1965 onwards may have not completely halted the progress of settlement in the structure. Nevertheless, this
441 resemblance motivates the use of this measured profile as a basis in the parametric investigation carried out in this
442 section.

443 The results of the parametric investigation are illustrated in Figure 14. They are presented in terms of the width
444 of cracks 2 and 3 vs. settlement of pillar 2, above which the cracks in question are situated. Initially, the Young's
445 modulus of the pillar was investigated, due to the initially determined value being higher than expected given the
446 compressive strength of the pillar masonry (see Table 1). The change in the Young's modulus of the pillar does
447 not significantly affect the response of the nave, due to the limited extent of the nave area in which it is encountered.
448 However, the reduction of the Young's modulus of the wall increases both the width of the cracks and the amount
449 of settlement of pillar 2. Interestingly, the reduction of the Young's modulus causes crack 2 to increase in width
450 and crack 3 to be severely reduced, owing to the redistribution of forces in the wall. Cracks 2 and 3 are differently
451 affected by changes in the tensile strength of the wall masonry as well. The width of crack 2 slightly increases for
452 any change in the parameter, while crack 3 decreases, practically disappearing for a decrease in the tensile strength.
453 Finally, the response was not particularly sensitive to changes in the tensile fracture energy of the wall masonry.
454 However, a slight increase in the total settlement of the pillar is registered for a decreased value of this parameter.



455

456

457

458

459

460

461

462

463

464

465

466

Figure 14 Results of parametric investigation: a) & b) Crack width for variation of Young's modulus, c) & d) crack width for variation of tensile strength, e) & f) crack width for variation of tensile fracture energy.

The results are also tabulated in Table 2, with the addition of the results of the horizontal movement and vertical settlement of pillar 2. The changes in the horizontal movement of the pillar, measured at the capital and indicating tilting rather than whole body slipping, are either associated with the crack widths above the pillar or with the capacity of the wall for post-cracking deformation (as influenced by an increase in the fracture energy).

Crack 2 did not present strong sensitivity to the material properties. Crack 3 presented some sensitivity to the tensile strength of masonry. The dependence on the Young's modulus of masonry is partially related to the increase of crack width due to reduced stiffness of the superstructure. The tensile fracture energy had only a marginal effect on either crack. The crack arrangement was not sensitive to the material properties. These observations suggest

467 that crack formation and development are more sensitive to the applied deformation profile. This outcome
 468 illustrates the importance of an accurate calculation of the properties of the soil and a good measurement of the
 469 historic settlement profile in order to achieve meaningful analysis results. In light of the envisaged intervention
 470 project, consolidation of the wall masonry, which would lead to some degree of increase of the tensile strength,
 471 fracture energy and Young's modulus of the material, can be beneficial in itself for maintaining the integrity of
 472 the church and limiting the effects of possible future differential settlement. This can act as a complement to the
 473 foundation strengthening and soil consolidation underway.

474 **Table 2 Results of parametric investigation. Percentile differences from reference model results in**
 475 **crack width and displacement (vertical and horizontal) of pillar 2.**

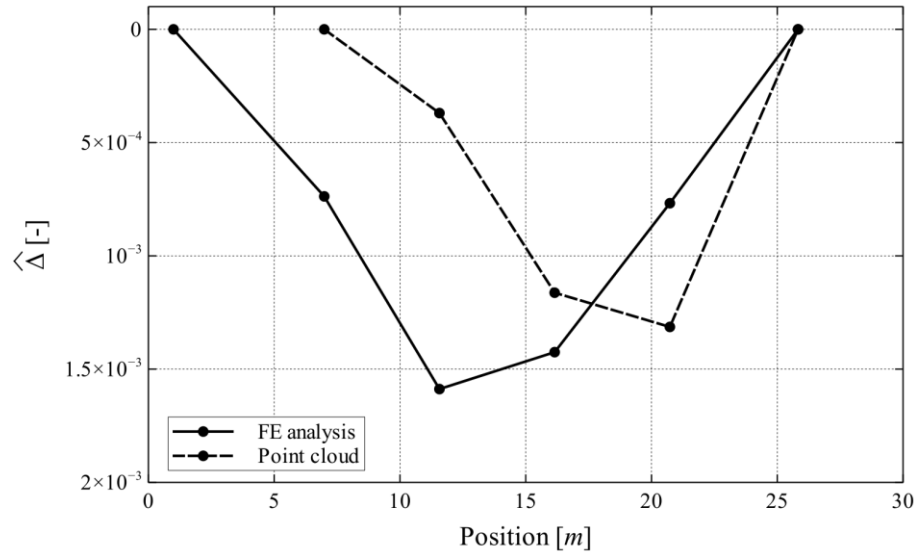
	Crack width 2	Crack width 3	$\Delta x_{pillar\ 2}$	$\Delta y_{pillar\ 2}$
Reference	100	100	100	100
$1/2 f_t$	146	32	190	105
$2f_t$	129	77	85	93
$1/2 G_f$	129	137	76	99
$2G_f$	83	105	271	91
$2/3 E_{pillar}$	85	111	97	103
$1/2 E_{pillar}$	80	136	102	107
$1/2 E_{wall}$	218	29	352	134

476 4.4 Discussion on Model Results

477 A final appraisal of the obtained results from the modeling approaches is warranted. In particular, the results
 478 from the phased analysis need to be contrasted with the monitoring and survey data. The final deformation profile
 479 obtained for the phased analysis (Figure 11) relies on the estimation of the behavior of the soil through time. The
 480 profile estimated from the architectural features of the building (Figure 6) depicts the effects of soil-structure
 481 interaction more directly. The latter profile compares favorably with the deformation profile obtained from
 482 monitoring data over the period 1994-2005. The normalization of the estimated settlements by disregarding the
 483 tower movement prior to the construction of the nave wall makes a direct comparison difficult. The lack of
 484 measurements in the period 2005-2018 further complicates matters, which the new intervention project will help
 485 clarify. Finally, the analysis approach does not take into account the full three-dimensional geometry effects of the

486 structure. These are potentially more acute near the crossing pillar due to the presence of the transept. Nevertheless,
487 the numerical analysis approach adopted here is able to capture the response of the nave with significant fidelity.

488 The assumption of a uniform interface stiffness below all the pillars in the nave is a necessary simplification
489 due to the lack of more detailed data. Despite resulting in an accurate crack pattern, the final disposition is not in
490 complete agreement with the settlement as estimated from the architectural feature analysis. However, a clearer
491 relation between the numerical and measured deformation profile is obtained when comparing deflection ratios.
492 The deflection ratio is defined as the ratio of the relative settlement to the length of the deflected part. In Figure
493 15, the deflection ratios along feature Line 4 (base of the pillar abacus of the first level) are presented, based on
494 the measurements shown in Figure 6. The deflection ratio along this line could be more clearly defined along a
495 larger portion of the structure compared to other lines and is sufficiently close to the base of the pillars to provide
496 an indication of the settlement. As Figure 15 illustrates, the deflection ratios between the two approaches are quite
497 similar, with the sagging of the colonnade between the tower and the crossing pillar being clearly indicated.



499

500 **Figure 15 Comparison of deflection ratio from finite element analysis and architectural feature**
 501 **measurement on the point cloud (Line 4).**

502 **5. Damage Calculation Using an Analytical Damage Function**

503 **5.1 Calculation of Model Parameters**

504 The model proposed by Giardina et al [7], which introduced an analytical relation between settlement and
 505 damage index for masonry buildings, will be adopted for the present study. The model relates the deflection ratio
 506 $\hat{\Delta}$ due to sagging or hogging ground deformation to a damage level of the structure according to the classification
 507 proposed by Burland & Wroth [23]. The damage level, linked to the severity of damage and the means required
 508 for its repair, is quantitatively expressed in terms of crack width, thus directly comparable to both documented
 509 pathology and nonlinear finite element analysis results. The damage classes are outlined in Table 3. The damage
 510 model for two-dimensional structures is a function of several geometric and material parameters expressed in a
 511 polynomial equation as follows:

$$d'_{2D}(\hat{\Delta}, \bar{x}) = d_{2D,ref}(\hat{\Delta}) + \sum_{i=1}^6 a_i \bar{x}_i = b_1 + b_2 \hat{\Delta} + b_3 \hat{\Delta}^2 + b_4 \hat{\Delta}^3 + \sum_{i=1}^6 a_i \bar{x}_i \quad (7)$$

512 where $d_{2D,ref}$ are the selected reference values, a_i and b_i are fitted polynomial coefficients and \bar{x} contains the
 513 normalized values of the model parameters x_i . The x_i model parameters, along with their reference values $x_{i,ref}$
 514 are given in Table 4. All values for the polynomial coefficients and the normalization process for the model
 515 parameters are detailed in [7]. From the value of the damage level calculated from the model, one can calculate
 516 the corresponding crack width through linear interpolation based on the values found in Table 3.

517 **Table 3 Damage classification for masonry structures subjected to differential settlements [23].**

Damage Level	Damage Class	Crack Width [mm]
1	Negligible	0.0 – 0.1
2	Very Slight	0.1 – 1.0
3	Slight	1.0 – 5.0
4	Moderate	5.0 – 15.0
5	Severe	15.0 – 25.0
6	Very Severe	>25.0

518 **Table 4 Damage model reference values $x_{i,ref}$ [7] and input for current analysis x_i .**

Openings	G_f	E	f_t	k_n	Interface shear behavior/Trough shape
[%]	[N/m]	[N/mm ²]	[N/mm ²]	[N/mm ³]	[-]
$x_{1,ref} = 30$	$x_{2,ref} = 10$	$x_{3,ref} = 3000$	$x_{4,ref} = 0.10$	$x_{5,ref} = 0.7 \times 10^9$	$x_{6,ref} = 1$
$x_1 = 31.92 \div 33.88$	$x_2 = 12$	$x_3 = 3000$	$x_4 = 0.10$	$x_5 = [\text{See Table 5}]$	$x_6 = 1$

519 Parameters x_1 to x_4 are derived according to the material properties used in the finite element analysis and the
 520 geometry of the nave. Parameter x_6 is assigned its reference value according to [7]. Special attention is drawn to
 521 the parameter x_5 related to the normal stiffness of the soil-structure interface. The reference value for x_5 has been
 522 calculated according to typical Dutch pile foundation systems distributed along the façade of brick masonry
 523 structures [24]. In the present research, this parameter is calculated from the modulus of subgrade reaction under
 524 vertical loading of the foundation system of the nave, an approach that generalizes the applicability of the damage
 525 function to other foundation and soil types. This approach additionally allows for taking into account foundation
 526 strengthening, micro-piling and foundation soil improvement directly in the damage function.

527 For strip foundations, the modulus of subgrade reaction k_n is directly equivalent to the parameter x_5 and can
 528 be applied to continuous shallow foundations of masonry walls. Equations for its calculation are available in the
 529 literature (e.g. [25,26]). Some further manipulation is required in the case of colonnades founded on individual
 530 footings, as is the case with the nave pillars of the present case study. The x_5 parameter for a series of m single
 531 footings j is then calculated as follows:

$$k_n = \frac{\sum_{j=1}^m k_n^j A_f^j}{\sum_{j=1}^m A_f^j} = x_5 \quad (8)$$

532 where k_n^j is the modulus of subgrade reaction of footing j . This can be calculated from equations (3) and (4)
 533 or from equations (4) and (5) if the settlement has been pre-estimated. This averaging approach to the subgrade
 534 reaction modulus is similar to the one followed for the allocation of the stiffness provided by the distributed piles
 535 according to Rots [24], but can be generalized as shown for continuous footings of walls or isolated footings of
 536 colonnades. This parameter becomes significant in light of the results shown in Figure 11. Despite the decrease in
 537 the deflection ratio as the phases progress, the damage, in terms of crack width, increases. This is captured by the
 538 damage model through the change in the x_5 parameter due to soil-structure interaction (decrease of the apparent
 539 Young's modulus of the foundation soil within a single phase). The disposition of the data points, capable of being
 540 approximated by a third order polynomial fit, suggests that the damage model can be successfully adapted to this
 541 case.

542 In addition to adjusting the reference value for the vertical interface stiffness (x_5), the a_5 coefficient associated
 543 with the interface stiffness is also adapted. These parameters are modified in order to fit the available numerical
 544 results of the phased analysis (phase B and C) and the reference model. The material properties of masonry are
 545 taken as equal to those of the wall masonry (Table 1), which comprises most of the structure and on which the
 546 majority of the damage is accumulated. The percentage of openings varies between 33.88% in phase B and 31.92%
 547 in phase C and the reference model.

548 **5.2 Results**

549 Using equation (8) the values for the parameter x_5 are found for the colonnade. These are shown in Table 5,
550 where it becomes apparent that the range of the parameter values varies within the range initially investigated in
551 [7], with the exception of the reference model case. Nevertheless, it is expected that the calibrated values for the
552 numerical model parameters be significantly different from those initially proposed. This is due to the fact that the
553 initial model was calibrated against a finite element benchmark where the interface stiffness was not extensively
554 investigated. A complete recalibration of the model is bound to alter the numerical parameters to some degree.

555 The slight increase of x_5 during the transition from long-term phase B to short-term phase C is contrary to the
556 progress of soil consolidation, which decreases the apparent short-term Young's modulus of the soil. However,
557 depending on the calculation method elected (such as for the estimated settlement method employed here or for
558 continuous footings), the x_5 parameter may depend directly or indirectly on the stiffness of the superstructure as
559 well. This stiffness is increased by the addition of the second level of the nave wall. This fact clearly illustrates the
560 significance of soil-structure interaction in the study of differential settlement damage problems.

561 The analytical model, when used with its initial reference values and normalization process, greatly
562 exaggerates the damage corresponding to the reference model and underestimates the damage in the phased
563 analysis (phases B and C). The calibration of the new parameters is performed by a simple minimization process,
564 during which the linear regression between FE and analytical crack widths is required to be a unitary slope curve.
565 The normalization of the x_5 parameter in [7] is carried out according to:

$$\bar{x}_5 = \frac{\log_{10} x_5 - \log_{10} x_{5,ref}}{2} \quad (9)$$

566 A new normalization of the parameters is proposed here in order to match the trend of interface stiffness to
567 damage level, according to which the \bar{x}_5 parameter is equal to:

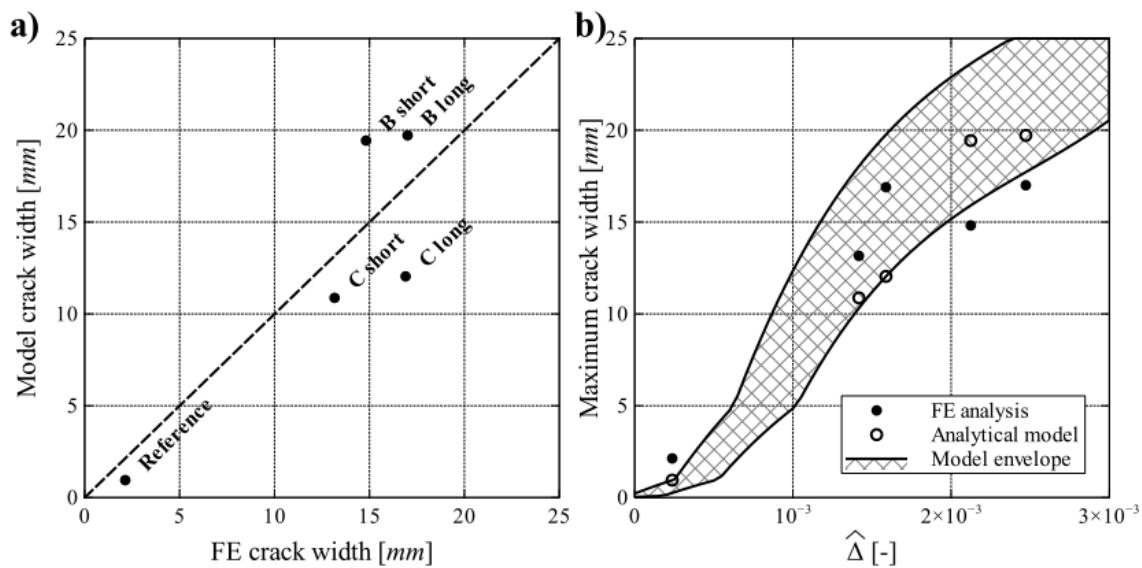
$$\bar{x}_5 = \left(\frac{\log_{10} x_{5,ref}}{\log_{10} x_5} \right)^{1.5} \quad (10)$$

568 The results of the modified analytical model are compared with the finite element analysis results in terms of
 569 the main cracks of the first level of the nave wall, following their calculation as described in the phased analysis
 570 section. The minimization process for the available data set produces a value for the a_5 parameter equal to -1.1722.
 571 The comparison of the results is plotted in Figure 16a, in which satisfactory agreement is found throughout the
 572 range of available data. Despite some discrepancy in the results in terms of crack width, the damage level is well
 573 approximated by the calibrated model.

574 **Table 5** x_5 parameter results for phase B model, phase C model and reference model.

	Reference	B short	B long	C short	C long
x_5 [N/mm ³]	1.43E+10	2.79E+07	9.63E+06	9.70E+06	6.86E+06

575 The envelope indicating the change in the polynomial model curve, almost entirely due to alterations in the
 576 spring stiffness and to a very minor extent due to changes in the opening percentage, is presented in Figure 16b.
 577 The upper envelope curve corresponds to the maximum apparent stiffness associated with the reference model and
 578 the lower curve corresponds to the minimum apparent stiffness of the long-term part of phase C. This fact
 579 illustrates the influence of the foundation stiffness, and, by extension, the properties of the soil, on the behavior of
 580 complex structures.



581

582 **Figure 16 a) Comparison of analytical model with FE analysis results. Dashed diagonal indicates line**
 583 **of equality between FE analysis and analytical modeling. b) Crack width according to damage prediction**
 584 **model and comparison with FE analysis results.**

585 The initial results of this approach towards the extension of the predictive analytical model are promising. The
 586 generalization of this extension requires robust verification in order to recalculate the numerical coefficients of the
 587 model. Coupled experimental tests and parametric numerical analyses need to be developed, along the same lines
 588 of the prior development of the analytical model but attempting to include variations in the vertical stiffness of the
 589 foundation. This is likely to lead to modifications to all numerical parameters, unlike the simplified calibration
 590 approach adopted in this paper, where only the parameters linked with the vertical stiffness were modified.

591 6. Conclusions

592 In this study the behavior of a church nave wall subjected to ground deformation over an extended period of
 593 time is investigated. The problem is approached through single-phase and multi-phase finite element analysis. The
 594 paper demonstrates the importance of detailed modeling of the soil behavior over time, the soil-structure
 595 interaction and the accurate measurement of settlements for the analysis of complex structures subjected to soil
 596 movement. Through this investigation it is shown that the application of a single-phase analysis does not reliably
 597 provide the cracking pattern observed in the actual structure. The need to take into account construction phases

598 and changes in the soil stiffness is clearly shown, even when studying individual element ensembles, such as the
599 nave wall here investigated. The importance of detailed geometric and damage survey is also demonstrated.

600 The sensitivity analysis illustrates the predominance of the deformation profile, as influenced mainly by the
601 soil-structure interaction, in the disposition of the cracking pattern on the structure. Nevertheless, the width of the
602 cracks is strongly influenced by the material properties of the nave wall, as are the obtained settlements, although
603 to a lesser degree.

604 The phased analysis, taking into account changes in the behavior of the soil and alterations in the geometry of
605 the structure, provides a complete picture of the history of the nave's pathology. Different major cracks appear
606 and develop at different phases of the building, due to redistribution of the forces and changes in the stiffness of
607 the foundations.

608 An analytical model for the prediction of the damage level in masonry structures subjected to differential
609 settlements is adapted and expanded. Moving beyond the initial formulation of the model, a method for the direct
610 calculation of the normal stiffness of the structure is proposed. Following calibration of the numerical coefficients
611 linked to this stiffness, the results of the model are consistent with the numerical analysis results and the crack
612 state of the real structure. Further expansion of the model along the lines pursued here can greatly enhance the
613 potential for accurate analytical modeling of complex masonry structures.

614 **Acknowledgements**

615 The authors acknowledge the funding received by BRAIN.be, Belspo in support of the GEPATAR research
616 project (“GEotechnical and Patrimonial Archives Toolbox for ARchitectural conservation in Belgium”
617 BR/132/A6/Gepatar).

618 **References**

619 [1] A.R. Sánchez, R. Meli, M.M. Chávez, Structural Monitoring of the Mexico City Cathedral (1990-2014),
620 Int. J. Archit. Herit. 10 (2016) 254–268. doi:10.1080/15583058.2015.1113332.

- 621 [2] L. Giresini, Energy-based method for identifying vulnerable macro-elements in historic masonry churches,
622 Bull. Earthq. Eng. 14 (2016) 919–942. doi:10.1007/s10518-015-9854-7.
- 623 [3] F. Portioli, L. Cascini, Large displacement analysis of dry-jointed masonry structures subjected to
624 settlements using rigid block modelling, Eng. Struct. 148 (2017) 485–496.
625 doi:10.1016/j.engstruct.2017.06.073.
- 626 [4] S. Galassi, G. Misseri, L. Rovero, G. Tempesta, Failure modes prediction of masonry voussoir arches on
627 moving supports, Eng. Struct. 173 (2018) 706–717. doi:10.1016/j.engstruct.2018.07.015.
- 628 [5] P. Roca, M. Cervera, L. Pelà, R. Clemente, M. Chiumenti, Continuum FE models for the analysis of
629 Mallorca Cathedral, Eng. Struct. 46 (2013) 653–670. doi:10.1016/j.engstruct.2012.08.005.
- 630 [6] S. Saloustros, L. Pelà, P. Roca, J. Portal, Numerical analysis of structural damage in the church of the
631 Poblet Monastery, Eng. Fail. Anal. 48 (2015) 41–61. doi:10.1016/j.engfailanal.2014.10.015.
- 632 [7] G. Giardina, M. Hendriks, J.G. Rots, Damage Functions for the Vulnerability Assessment of Masonry
633 Buildings Subjected to Tunneling, J. Struct. Eng. 141 (2015) 1–13. doi:10.1061/(ASCE)ST.1943-
634 541X.0001162.
- 635 [8] D. Peduto, G. Nicodemo, J. Maccabiani, S. Ferlisi, Multi-scale analysis of settlement-induced building
636 damage using damage surveys and DInSAR data: A case study in The Netherlands, Eng. Geol. 218 (2017)
637 117–133. doi:10.1016/j.enggeo.2016.12.018.
- 638 [9] D. Peduto, S. Ferlisi, G. Nicodemo, D. Reale, G. Pisciotta, G. Gullà, Empirical fragility and vulnerability
639 curves for buildings exposed to slow-moving landslides at medium and large scales, Landslides. 14 (2017)
640 1993–2007. doi:10.1007/s10346-017-0826-7.
- 641 [10] L. Schueremans, K. Van Balen, K. Brosens, D. Van Gemert, P. Smars, The Church of Saint-James at
642 Leuven: Structural Assessment and Consolidation Measures, Int. J. Archit. Herit. 1 (2007) 82–107.

- 643 doi:10.1080/15583050601126137.
- 644 [11] S. Sanchez-Beitia, L. Schueremans, K. Van Balen, On-site stress measurement on the piers of the Saint
645 Jacobs church in Leuven, Belgium, *Int. J. Archit. Herit.* 3 (2009) 110–125.
646 doi:10.1080/15583050802278794.
- 647 [12] E. Verstrynge, L. Schueremans, P. Smars, Controlled Intervention: Monitoring the Dismantlement and
648 Reconstruction of the Flying Buttresses of Two Gothic Churches, *Int. J. Archit. Herit.* 6 (2012) 689–708.
- 649 [13] G. Heirman, K. Brosens, Uitvoeringsdossier Globale Stabiliteitswerken Sint-Jacobskerk. Internal report
650 D/0800/10, Triconsult nv, 2017.
- 651 [14] M. Bassier, G. Hardy, L.-E. Bejarano-Urrego, A. Drougkas, E. Verstrynge, K. Van Balen, M. Vergauwen,
652 Semi-automated creation of accurate FEM meshes of heritage masonry walls from point cloud data, in:
653 11th Int. Conf. Struct. Anal. Hist. Constr. Cusco, Peru, 2019: pp. 305–314.
- 654 [15] K. Van Balen, K. Nuyts, P. Smars, D. Van de Vijver, Optimalisatie van standzekerheidsmodellen van
655 gewelfde gotische structuren gebruik makend van informatie uit vervormingsmetingen en scheuranalyse.
656 Internal report PV30318, KU Leuven, 1995.
- 657 [16] A.W. Koppejan, A formula combining the Terzaghi load compression relationship and the Buisman secular
658 time effect, in: *Proc. 2nd Int. Conf. Soil Mech. Found. Eng.*, 1948: pp. 32–38.
- 659 [17] G. Giardina, A. V van de Graaf, M. Hendriks, J.G. Rots, A. Marini, Numerical analysis of a masonry façade
660 subject to tunnelling-induced settlements, *Eng. Struct.* 54 (2013) 234–247.
661 doi:10.1016/j.engstruct.2013.03.055.
- 662 [18] A. Drougkas, P. Roca, C. Molins, Numerical prediction of the behavior, strength and elasticity of masonry
663 in compression, *Eng. Struct.* 90 (2015) 15–28. doi:10.1016/j.engstruct.2015.02.011.
- 664 [19] R. De Borst, Smearred cracking, plasticity, creep, and thermal loading—A unified approach, *Comput.*

- 665 Methods Appl. Mech. Eng. 62 (1987) 89–110.
- 666 [20] H.W. Reinhardt, Fracture Mechanics of an Elastic Softening Material Like Concrete., *Heron*. 29 (1984) 1–
667 42. doi:10.1023/A:1012235530463.
- 668 [21] G. Gazetas, Foundation Vibrations, in: H.-Y. Fang (Ed.), *Found. Eng. Handb.*, 1991: pp. 553–593.
669 doi:10.1007/978-1-4615-3928-5_15.
- 670 [22] TNO, DIANA Finite Element Analysis, User’s Manual, (2017).
- 671 [23] J.B. Burland, C.P. Wroth, Settlement of buildings and associated damage, in: *Settl. Struct. Proc. Conf. Br.*
672 *Geotech. Soc.*, 1974: pp. 611–764.
- 673 [24] J.G. Rots, Settlement Damage Predictions For Masonry, in: *Maint. Restrengthening Mater. Struct. Brick*
674 *Brickwork Proc. Int. Work. Urban Herit. Build. Maint. IV*, 2000: pp. 47–62.
- 675 [25] M.A. Biot, Bending of an infinite beam on an elastic foundation, *J. Appl. Math. Mech.* 2 (1937) 165–184.
676 doi:10.1016/0021-8928(58)90136-9.
- 677 [26] A.B. Vesić, Beams on Elastic Subgrade and the Winkler’s Hypothesis, in: *Proc. 5th Int. Conf. Soil Mech.*
678 *Found. Eng. Paris, Fr.*, 1961: pp. 845–850.
- 679